

# AN OPTICAL COMPARISON OF SILICONE AND EVA ENCAPSULANTS FOR CONVENTIONAL SILICON PV MODULES: A RAY-TRACING STUDY

Keith R. McIntosh,<sup>1</sup> James N. Cotsell,<sup>1</sup> Jeff S. Cumpston,<sup>1</sup>  
Ann W. Norris,<sup>2</sup> Nick E. Powell,<sup>2</sup> and Barry M. Ketola<sup>2</sup>

<sup>1</sup>Centre for Sustainable Energy Systems, Australian National University, Canberra, ACT 0200, AUSTRALIA

<sup>2</sup>Dow Corning Corporation, Midland, Michigan 48686, USA

Tel: +61-2-6125-8966, Fax: +61-2-6125-8873, Email: keith.mcintosh@anu.edu.au

## ABSTRACT

Ray-trace simulation is used to quantify the optical losses of photovoltaic modules containing silicon cells. The simulations show that when the module's encapsulant is silicone rather than ethylene vinyl acetate (EVA), the module's short-circuit current density under the AM1-5g spectrum is 0.7–1.1% higher for screen-printed multi-cSi cells, 0.5–1.2% higher for screen-printed mono-cSi cells, and 1.0–1.6% higher for high-efficiency rear-contact cells, depending on the type of silicone. This increase is primarily due to the transmission of short-wavelength light (<420 nm) and is therefore greatest when used with low UV-absorbing glass and cells of a high IQE at short wavelength. We also quantify absorption in the glass, EVA and silicone at longer wavelengths and describe the influence of an encapsulant's refractive index on escape losses.

## INTRODUCTION

The encapsulant used in a photovoltaic (PV) module has many requirements. It must be optically transparent, electrically insulating, mechanically compliant, adherent to both glass and cells, and sufficiently robust to withstand 20–30 years in the field. Since the early 1980s, the encapsulant in almost all PV modules has been ethylene vinyl acetate (EVA). Therefore, it is the benchmark with which to compare other materials.

An optically superior alternative to EVA is silicone [1–4]. The advantage of employing silicone rather than

EVA has been quantified in several recent studies in terms of a module's short-circuit current density  $J_{sc}$  under the AM1-5g spectrum: Ketola *et al.* measured a 1.5% advantage in single-cell modules containing SunPower-type rear-contact cells [1], Ohl and Hahn calculated a 0.76–1.0% advantage from EQE curves of encapsulated screen-printed cells [2], and Kempe calculated a 0.5% advantage from transmission measurements of glass-encapsulant-glass sandwiches [3]. These comparative studies are somewhat incomplete, however, as they do not quantify the behavior of full PV modules (an expensive undertaking given the large number of modules required to resolve statistical variation).

An accurate optical assessment of a PV module is not trivial. As illustrated by Figure 1, incident rays reflect from the air-glass (1), glass-encapsulant (3), encapsulant-cell (6) and encapsulant-backsheet (8) interfaces; and in the latter two cases, the reflection is often diffuse, leading to some of the reflected light being total-internally reflected at the glass-air interface and then returned to the cells. Furthermore, incident rays are absorbed in the glass (2), the encapsulant (4), the cell's antireflection coating or metal fingers (5), and the backsheet (7). These eight interactions depend on the light's incident wavelength and incident angle. Therefore, a comprehensive optical assessment is aided by the application of ray tracing.

This paper presents the results of ray-trace simulations of conventional PV modules fabricated from three types of silicon cells, where the encapsulant is either EVA or one of three silicones. It begins with an assessment of the optical parameters of the module components.

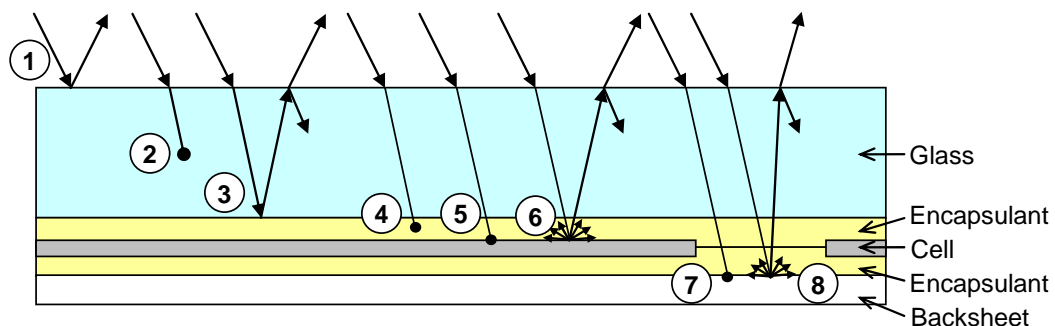


**Figure 1:** Cross-sectional diagram of a conventional PV module (to scale), and the optical loss mechanisms as listed in the text.

## REFRACTIVE INDEX AND ABSORPTION COEFFICIENT OF ENCAPSULANTS AND GLASS

Figure 2 plots (a) the real refractive index  $n$  and (b) the absorption coefficient  $\alpha$  of five materials as a function of wavelength  $\lambda$ . These include three silicones developed by Dow Corning Corporation, dubbed 201, 203 and 205 in this paper; they were chosen to cover a wide range of refractive index while maintaining low absorption. The figure also includes data for conventional EVA attained from STR Solar and low-iron Starphire® glass from PPG, where the glass was the least absorptive of many assessed during this project. All data was experimentally determined by the procedure outlined in the appendix of Reference [5].

Figure 2(a) illustrates the dispersion of the materials (i.e., the variation of  $n$  with  $\lambda$ ). For the glass, the slope and magnitude agree well with those of Rubin [6] but less so with those of Nagel *et al.* [7]. For the silicones, we attained near-identical data for  $n(\lambda)$  from spectroscopic ellipsometry on very thin samples, though over a smaller wavelength range. And for the EVA, we found no published data with which to compare our measurements of  $n(\lambda)$ . In this instance, we neglect the results of Nagel *et al.* who determined  $n(\lambda)$  from glass–EVA–glass sandwiches (rather than free-standing EVA samples), and therefore could not distinguish subtle differences in  $n(\lambda)$  between the glass and EVA.

Although the simulations that follow employ the experimental data of Figure 2(a) we also provide a parameterisation of the data. Table I lists the best-fit data and its uncertainty to 95% confidence of a least-squares fit to the first three terms of the Schott dispersion formula [8],

$$n(\lambda) = a + b\lambda^2 + c\lambda^{-2} + d\lambda^{-4} + \dots, \quad (1)$$

over the range, 300–1600 nm. The Schott formula provides a reasonable compromise between simplicity and accuracy, where the accuracy can be assessed by the chi-squared listed in the table. In a future work we will provide the best-fit parameters to the Sellmeier formula, which is more complicated but a better physical representation of dispersion.

Figure 2(a) shows that  $n(\lambda)$  of EVA is similar to that of glass, leading to near-ideal optical coupling between the materials. By contrast,  $n(\lambda)$  of silicone 201, which is typical of most silicones, is notably lower than  $n(\lambda)$  of glass. This leads to a small reflection at the glass–silicone interface and, more importantly, to an increase in the light that escapes after diffuse reflection from the backsheet. Such losses are described in more detail below. Figure 2(a) also indicates that higher  $n(\lambda)$  was achieved by silicones 203 and 205, this data shows the wide range in  $n$  which can be obtained for silicones.

Figure 2(b) indicates that the short-wavelength absorption of EVA extends to 417 nm (agreeing well with Nagel *et al.* [7]), compared to 273 nm, 315 nm and 330 nm for silicones 201, 203 and 205, respectively. Here, we have arbitrarily defined this ‘cut-off’ wavelength to be where absorption descends below 1% of incident photons

for 450  $\mu\text{m}$  of encapsulant (i.e., the typical thickness of one sheet of EVA). Thus, the silicones transmit significantly more short-wavelength photons than EVA, and while the AM 1.5G spectrum contains diminishing amounts of photons below 417 nm, it still remains a significant advantage for silicones. It is this difference that has been the focus of previous studies [2, 3].

The relative advantage of silicone over EVA depends strongly on the cut-off wavelength of the glass: a high transmission is of no value if the light has already been absorbed by an overlying material. In glass, the cut-off wavelength depends strongly on its cerium and iron contents. The cut-off wavelength was found to be 330 nm for the low-iron Starphire®, which compares well to many other PV glasses but is greater than can be attained by replacing the cerium with antimony.

Figure 2(b) shows that all of the encapsulants exhibit absorption peaks at 900–940 nm, 1000–1050 nm and 1100–1300 nm, which are attributable to C-H absorptions due to vibrational overtones. We have not found previously published data on EVA’s  $\alpha(\lambda)$  at wavelengths greater than  $\sim 400$  nm, so it is interesting to note that its absorption peaks have a similar magnitude to those of silicone but are broader and centred at a longer wavelength ( $\sim 20$  nm). The figure indicates that with 450  $\mu\text{m}$  of encapsulant, the first two peaks absorb between 0.1% and 0.9% of incident photons, while the latter absorbs up to 8%. The resulting losses for modules fabricated from silicon cells are small but not negligible, as quantified later in the paper.

Finally, we note that in Figure 2(b),  $\alpha(\lambda)$  is higher for EVA than for silicone over the wavelength range, 400–850 nm. In fact, this  $\alpha(\lambda)$  is the lowest we have observed of 13 samples prepared from the same EVA. Nevertheless, it is uncertain whether the results of both the EVA and silicone overestimate the true absorption in this wavelength range due to scattering within the encapsulant—the subject of a future study.

## INPUTS AND ASSUMPTIONS

We simulate 12 modules fabricated from three types of cells: (A) planar multi-cSi screen-printed cells, (B) textured mono-cSi screen-printed cells, and (C) textured mono-cSi rear-contact cells. Types A and B are typical of those manufactured by many screen-print manufacturers, and type C is typical of those manufactured by SunPower Corporation [9]. We use the dimensions defined in Figure 3 and listed in Table II.

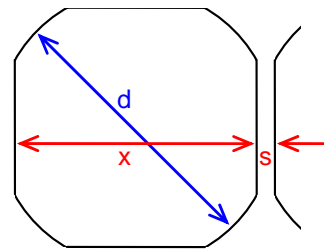


Figure 3: Cell dimensions.

**Table I:** Least-squares fit of the Schott dispersion formula to empirical data, where the uncertainty represents a 95% confidence interval.

material	$a$	$b$ (nm <sup>-2</sup> )	$c$ (nm <sup>2</sup> )	$\chi^2$	ref
201	1.3985 ± 0.0003	-3.8 ± 0.2 × 10 <sup>-9</sup>	38.6 ± 0.5 × 10 <sup>2</sup>	8 × 10 <sup>-6</sup>	
203	1.4506 ± 0.0003	-1.1 ± 0.2 × 10 <sup>-9</sup>	78.6 ± 0.6 × 10 <sup>2</sup>	10 × 10 <sup>-6</sup>	
205	1.5241 ± 0.0005	-0.5 ± 0.3 × 10 <sup>-9</sup>	116.3 ± 0.9 × 10 <sup>2</sup>	30 × 10 <sup>-6</sup>	
EVA	1.4830 ± 0.0001	-4.5 ± 0.1 × 10 <sup>-9</sup>	33.9 ± 0.3 × 10 <sup>2</sup>	3 × 10 <sup>-6</sup>	
low-Fe glass	1.5048 ± 0.0003	-3.0 ± 0.2 × 10 <sup>-9</sup>	21.1 ± 0.6 × 10 <sup>2</sup>	1 × 10 <sup>-6</sup>	
sodalime glass	1.513	-3.2 × 10 <sup>-9</sup>	39.6 × 10 <sup>2</sup>		[6]

**Table II:** Dimensions of cells within modules. (Metal fraction refers to cell area not module area.)

Cell type	Cell dimensions							Finger dims.		Busbar dims.		Metal fraction	
	Surface	c-Si	Metal	x (cm)	d (cm)	A (cm <sup>2</sup> )	s (cm)	Packing factor	Width (mm)	Separatn (mm)	Number		Width (mm)
A	planar	multi	screen-printed	15.6	22.5	243.4	0.2	97.5%	0.12	2.3	2	2	7.4%
B	textured	mono	screen-printed	15.6	19.5	236.5	0.2	94.7%	0.12	2.3	2	2	7.5%
C	textured	mono	rear-contact	12.5	15.0	148.6	0.2	92.1%	-	-	-	-	0.0%

**Table III:** material properties; note that  $k = \alpha\lambda / 4\pi$ .

Material	thickness	$n(\lambda)$ and $k(\lambda)$	Notes
Glass	3 mm	Fig. 2	low-iron, Ce doped
Encapsulant	450 $\mu$ m	Fig. 2	
SiN <sub>x</sub> ARC	optimised	Fig. 4	Varies from one manufacturer to another
SiO <sub>2</sub>	20 nm	[11]	Relevant to type C only
Si	n.a.	[12]	
Ag	n.a.	[11]	Screen-print fingers assumed to be pure Ag

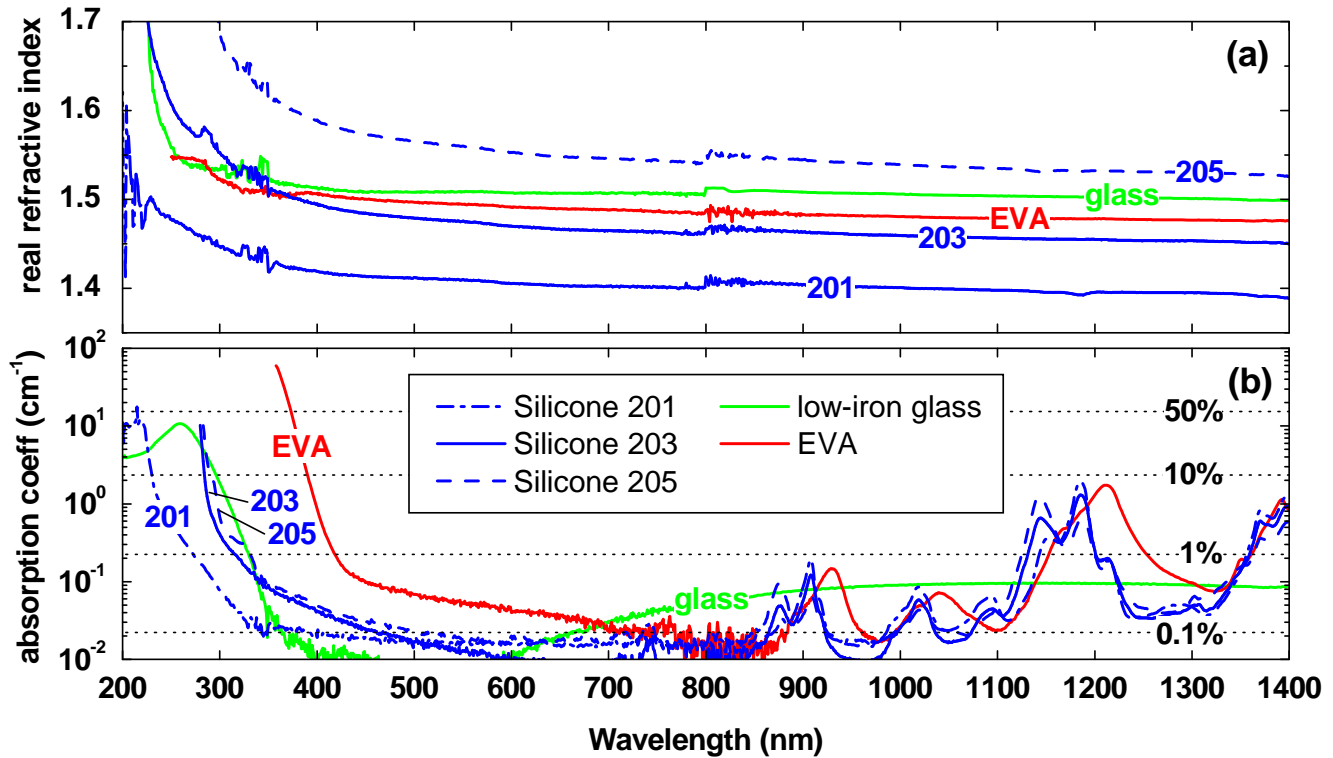


**Figure 2:** (a) Real refractive index and (b) absorption coefficient as a function of wavelength for STR's EVA, PPG's low-iron Starphire® glass, and Dow Corning's silicones 201, 203 and 205. The dotted lines in Figure 2(b) show the percentage of light that is absorbed by 450  $\mu$ m of material (typical thickness of EVA). Best viewed in colour.

Figure 5(a) plots the IQE of the cells when encapsulated in EVA. The data for types A and B was attained from experimental measurements of recent production-grade cells, while the data for type C is several years old and slightly inferior to those of more recent rear-contact cells. In all cases the measurements were conducted by major cell manufacturers on their unencapsulated cells and they include absorption in the antireflection coating (ARC), as is conventional. Since absorption in the ARC changes after encapsulation depending on the refractive index of that encapsulation, we modified the IQE accordingly in each simulation.

The absorption in—and the reflection from—the encapsulated cell's ARC was determined by the transfer matrix method [10]. Table III presents the thickness of the materials and the source of the real  $n(\lambda)$  and imaginary  $k(\lambda)$  refractive index used in the calculations. All light was assumed normally incident with equal components of TM and TE polarisation. For the textured cells, which have pyramidal texture, the calculation of absorption and reflection took into consideration the first and second bounces that normally incident light makes on pyramidal texture [13]: the first at an incident angle of  $54.75^\circ$  and the second at  $15.75^\circ$ . Figure 5(b) plots the reflection when encapsulated in EVA. It changes slightly when encapsulated by materials of another refractive index, as was accounted for in the simulations that follow. Note, however, that the thickness of the  $\text{SiN}_x$  ARC was adjusted to maximise the transmission of light into the cell. For the rear-contact cells (type C), the reflection and absorption were determined with a 20 nm  $\text{SiO}_2$  passivation layer between the  $\text{SiN}_x$  ARC and the Si [9]. The reflection was assumed specular from the planar cells and Lambertian from the textured cells; the latter is a poor approximation of the actual angular distribution of light reflected from randomly oriented upright pyramids but the approximation has little affect on the simulations as will be shown.

Reflection from the metal fingers was calculated in the same manner as from the ARC assuming them to be of pure silver. The results in EVA are plotted in Figure 5(b). In the cell types with metal fingers on the front surface (A and B), the reflection was assumed specular and the fingers were assumed to have zero thickness. Hence, the simulations did not account for rays that are obliquely reflected by the curvature of the fingers.

Reflection at the encapsulant–backsheet interface was taken from Shaw's internal reflection of Dupont™ Tedlar®, [14] plotted in Figure 5(b). We therefore assume the encapsulant has the same  $n(\lambda)$  as the backsheet. Our own measurements are consistent with Shaw, though determined by an alternative technique (the subject of another work). We assume Lambertian reflection from the backsheet with no light reflected onto the rear of the cells.

Reflection at the air–glass and glass–encapsulant interfaces was determined for every ray and accounts for changes in the angle of incidence. Reflection was assumed angle-independent, however, for intersections at the encapsulant–cell and encapsulant–backsheet interfaces. This introduces error due to the light that reflects back onto the cell after diffuse reflection, though it constitutes a small fraction of the losses.

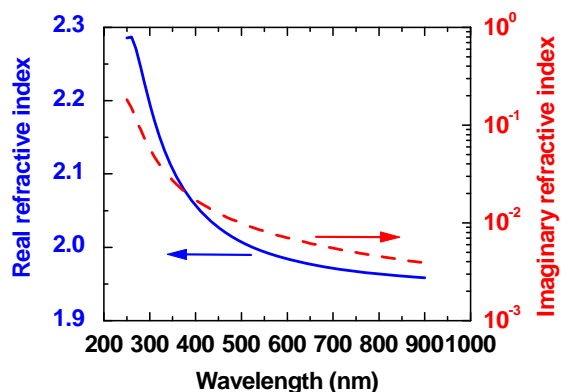


Figure 4: Experimentally measured refractive index of PECVD  $\text{SiN}_x$  deposited by a major manufacturer.

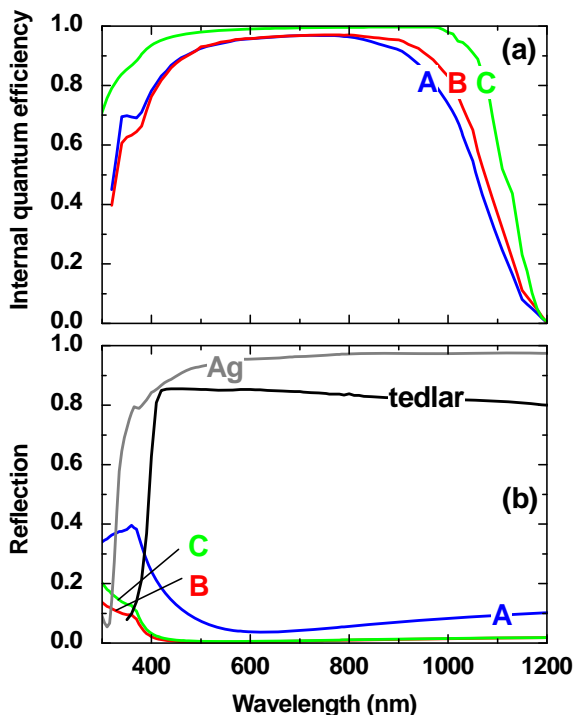


Figure 5: (a) IQE and (b) reflection from the ARC of cell types A, B and C when encapsulated in EVA; 3(b) includes reflection from Ag and Tedlar® when encapsulated by EVA.

The modules are assumed infinitely large (omits influence of module edges) with spatially uniform properties. Interfaces are assumed parallel and either specular or Lambertian. Scattering within materials is neglected, as are rays that escape from the cell.

Each simulation consists of a million rays representing  $100 \text{ mW/cm}^2$ , normally incident, AM1-5g illumination [15]. The associated uncertainty in  $J_{sc}$  was  $\pm 0.1\%$  or  $\pm 0.03 \text{ mA/cm}^2$ , well below that introduced by other factors described earlier. We do not believe, however, that these uncertainties significantly affect the relative comparison between silicone and EVA, which depends mostly on the short-wavelength transparency and backsheet reflection.

**Table IV:** Optical losses in terms of percentage of the ideal  $J_{sc}$ , where the ideal  $J_{sc}$  of type A is 38.3 mA/cm<sup>2</sup>, of type B is 39.2 mA/cm<sup>2</sup>, and of type C is 42.9 mA/cm<sup>2</sup>.

Loss mechanism	Cell Type A				Cell Type B				Cell Type C			
	EVA	201	203	205	EVA	201	203	205	EVA	201	203	205
Reflection from front	4.10	4.10	4.10	4.10	4.10	4.10	4.10	4.10	4.10	4.11	4.10	4.10
Absorption in glass	1.36	1.37	1.38	1.38	1.47	1.45	1.47	1.50	1.55	1.52	1.55	1.59
Absorption in encapsulant	1.61	0.13	0.11	0.14	1.42	0.14	0.11	0.15	1.81	0.15	0.13	0.17
Absorption in backsheet/metal	0.73	0.77	0.79	0.80	1.32	1.42	1.42	1.44	1.58	1.69	1.69	1.72
Escape loss	12.31	12.94	12.92	13.15	8.49	9.18	8.85	8.58	3.51	4.22	3.79	3.47

**Table V:** Absorption in glass and encapsulant within wavelength ranges for cell type C (data in mA/cm<sup>2</sup>).

Region	Range (nm)	glass*	EVA	201
Short-wavelength	< 420	0.026	0.675	0.003
Mid-wavelength	420–880	0.300	0.069	0.030
Smaller peaks	880–1100	0.320	0.027	0.025
Large peak	> 1100	0.020	0.005	0.006

\* In this table, glass absorption is specifically for an EVA-encapsulated module; it varies slightly for a silicone-encapsulated module due to secondary passes.

## RESULTS

Figure 6 summarises the results, plotting  $J_{sc}$  for modules of each cell type and encapsulant. There is a small but significant increase in  $J_{sc}$  when EVA is replaced by silicone, and when the refractive index of the encapsulant is increased (except cell type A).

Table IV quantifies the various optical losses, listing them as a percentage of the  $J_{sc}$  that would be attained if there had been no losses at all. This ideal  $J_{sc}$  is dictated by the spectrum and the cells' IQE and is listed in the table caption. The optical losses can be understood as follows.

### Reflection from front:

Reflection from the front of the module is 4.1% and identical for all modules. It is governed by the refractive index of the glass, which was the same in all cases.

### Absorption in glass:

Absorption in the glass increases slightly as the cell type changes from A to B to C (1.4% to 1.5% to 1.6%). Since the modules have the same glass, this difference is not due to the light's first pass through the module. Instead, the difference is due to the light's secondary passes after being reflected by the cell or backsheet. Secondary passes are greatest in modules with high reflection from the cells and backsheet, particularly when the reflection is diffuse due to its high fraction of oblique rays. The main reason for the increase in glass absorption is the decrease in packing factor (Table II), and therefore increase in backsheet area, leading to more light passing multiple times through the glass.

### Absorption in encapsulant:

Absorption in the encapsulant is remarkably small (<0.2%) for all modules containing silicone. By contrast, absorption in the EVA is significant (1.4–1.8%). Like glass, absorption in the encapsulant is greater when there are more secondary passes. There is a slightly different trend for the encapsulant than for the glass, however, due

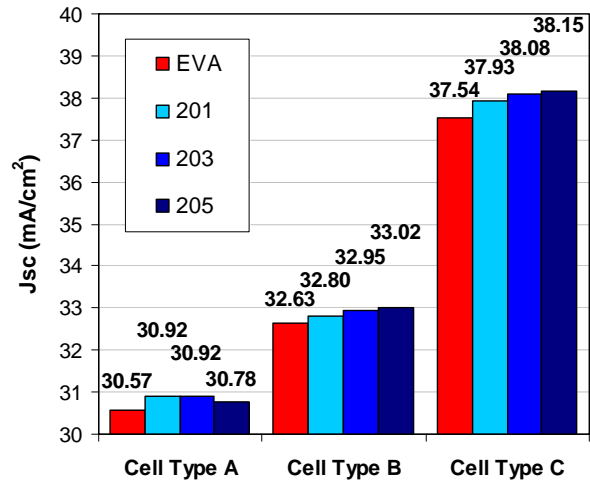


**Figure 6:** Results from ray-tracing study plotted in terms of the module's short-circuit current density.

to its stronger dependence on short-wavelength light, and to cell A's high reflection at short wavelength.

The dependence of the absorption on wavelength is summarised in Table V for cell type C. This cell has the highest IQE at all wavelengths and is therefore the most sensitive. The table indicates that at short wavelengths, EVA absorbs strongly, the glass slightly, and the silicone almost not at all. At longer wavelengths, the glass absorbs more strongly than the encapsulants due to the broad absorption peak associated with iron (Figure 2). As mentioned above, PPG's low-iron Starphire® glass had the lowest  $\alpha(\lambda)$  of all glass we examined, and hence, other glass would exhibit more absorption. For the encapsulants, the small and large absorption peaks absorb similarly, irrespective of whether they are EVA or silicone. Modules with high cell IQEs at long wavelengths are more affected by these peaks. Finally, we mention that the small absorption at mid-wavelengths in both the EVA and silicone could be an overestimate due to scattering affecting the measurement of  $\alpha(\lambda)$  when it is small.

### Absorption in the backsheet and metal:

Absorption in the backsheet is smaller for cells of less backsheet area (A, B then C), while absorption in the metal is greater for cells with more metal (A, B then C).

### Escape loss:

The escape loss is greatest for type A modules for two reasons: (i) being planar, the cells reflect in a specular

manner and hence light cannot be trapped within the module via total internal reflection (TIR) at the glass–air interface; and (ii) it has the highest reflection from the cells' ARC.

The escape loss for type B modules is smaller because being textured, reflection from the cells is less and diffuse (leading to TIR at the glass–air interface).

The escape loss for type C modules is smaller still because the cells have no metal on the front.

We note that these results overestimate the escape loss from cells with metal (A and B) because the simulations do not permit oblique reflection from any curvature in the fingers. The overestimation would have little effect on the relative comparison of EVA to silicone.

Table V shows that when the modules have a large diffuse area (B and C) the escape loss is smaller for encapsulants of a higher refractive index. This has little to do with reflection from the glass–encapsulant or encapsulant–ARC interfaces, which are both relatively small. Instead, it relates to diffuse reflection from the backsheet and cells and the subsequent TIR at the glass–air interface. Assuming Lambertian reflection, the fraction of light within the escape cone  $f_{esc}$  depends only on the refractive index of the encapsulant  $n_{enc}$  (and not the glass due to Snell's law) by the equation [16],

$$f_{esc} = \frac{2\pi \int_0^{\theta_c} \cos \theta \sin \theta d\theta}{2\pi \int_0^{\pi/2} \cos \theta \sin \theta d\theta} = \frac{1 - \cos 2\theta_c}{2} = \frac{1}{n_{enc}^2}, \quad (2)$$

where  $\theta_c$  is the critical angle.

Figure 7 plots  $f_{esc}(n_{enc})$ . It shows that as  $n_{enc}$  increases from 1.40 to 1.55,  $f_{esc}$  decreases from 0.51 to 0.42. This decrease in escape loss results in more TIR and therefore a higher  $J_{sc}$ , as evidenced by Figure 6 for the modules with more Lambertian surface (B and C). In both cases, ~90% of this benefit arises from reflection from the highly reflective backsheet and just ~10% from the lowly reflective cells (for which Lambertian reflection is a poor approximation). The source of the escape loss for type A was 51% fingers, 43% ARC, 6% backsheet; for type B was 73% fingers, 3% ARC, 24% backsheet; and for type C was 10% ARC, 90% backsheet.

For type A modules, which have planar cells and very little backsheet exposed, there is no advantage to using the silicones of higher refractive index. There is, in fact a slight disadvantage to using 205 due to more absorption.

Finally, we note that considerable improvement could be gained by encapsulants of still higher  $n$  (Fig. 7). These encapsulants need not be thick, but simply be adjacent to the Lambertian backsheet. If necessary, one might employ two encapsulants: a thin encapsulant of high  $n$  to coat the cells and backsheet, and another of lower  $n$  providing the bulk of the encapsulant and ensuring low  $\alpha$ .

## CONCLUSION

Ray-trace simulation was used to quantify the optical losses of three conventional PV modules. When the modules' encapsulant is silicone rather than EVA, there is a 0.9–1.6% increase in the module's  $J_{sc}$ . This increase is

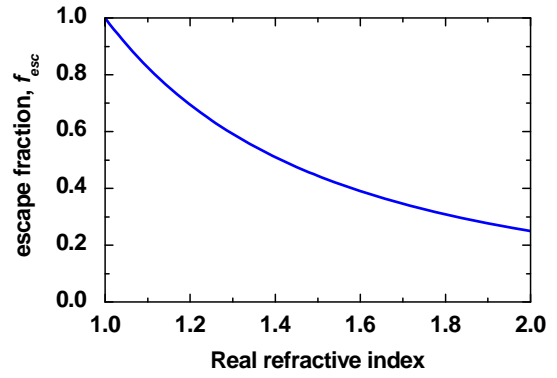


**Figure 7:** Fraction of light within the escape cone at the glass–air interface vs the encapsulant's refractive index for light reflected from a Lambertian backsheet

primarily due to the transmission of short-wavelength light (<420 nm), and is therefore greatest when used with low-absorbing glass and cells with a high IQE at short wavelength, such as rear-contact cells. The advantage remains significant, however, even when the cells are modern screen-printed multi-cSi cells.

We have also quantified absorption in low-iron Starphire® glass (1.5%), EVA (0.2%) and silicone (0.1%) at wavelengths greater than 420 nm. This absorption in the glass is strongly dependent on iron concentration [6] and could be significantly higher for other types of glass, even those classified as low-iron.

Finally, we have described the importance of the encapsulant's refractive index. Over the examined range, it has a little effect on reflection at the glass–encapsulant interface, a small effect at the encapsulant–cell interface, and a much larger effect on the escape fraction from Lambertian backsheets.

Thus, silicone is most preferable to EVA when (i) the cells have a high IQE at short wavelength, (ii) the silicone has a high refractive index, and (iii) there is a large exposed area of diffusely reflective backsheet.

## REFERENCES

- [1] B. Ketola *et al.*, *23rd EU PVSEC*, 2969 (2008).
- [2] M.D. Kempe, *33rd IEEE PVSC*, paper 421 (2008).
- [3] S. Ohi and G. Hahn, *23rd EU PVSEC*, 2693 (2008).
- [4] F. Dross *et al.*, *Sol. En. Mat. Cells* **90**, 2159 (2006).
- [5] K.R. McIntosh *et al.*, *Prog. Photovolt.* **17**, 191 (2009).
- [6] M. Rubin, *Sol. En. Mat.* **12**, 278 (1985).
- [7] H. Nagel *et al.*, *Prog. Photovolt.* **7**, 245 (1999).
- [8] H. Bach and N. Nuerth (Eds.), *The Properties of Optical Glass*, 2nd ed., Springer, Berlin, 25 (1995).
- [9] W.P. Mulligan *et al.*, *19th EU PVSEC*, 387 (2004).
- [10] H.A. Macleod, *Thin Film Optical Filters*, 2nd ed., Adam Hilger Ltd., Chapter 2 (1986).
- [11] E.D. Palik, ed., *Handbook of Optical Constants of Solids*, Vol. 1, Academic Press, Orlando (1985).
- [12] M.A. Green *et al.*, *Prog. Photovolt.* **3**, 189 (1995).
- [13] K.R. McIntosh *et al.*, accepted *J. Appl. Phys* (2009).
- [14] N.C. Shaw, PhD thesis, UNSW, 43–55 (2003).
- [15] International standard, IEC 60904-3, 2.0 (2008).
- [16] P. Campbell *et al.*, *J. Appl. Phys.* **62**, 243 (1987).